Theor Chem Acc (2012) 131:1281
DOI 10.1007/s00214-012-1281-0

REGULAR ARTICLE

Extensive theoretical investigation: influence of the electrostatic environment on the $I_3^-\cdots I_3^-$ anion–anion interaction

Ferdinand Groenewald · Catharine Esterhuysen · Jan Dillen

Received: 18 July 2012 / Accepted: 14 September 2012 / Published online: 2 October 2012

Abstract A theoretical study of the triiodide ion and $I_3^-\cdots I_3^-$ interactions in the dimer was performed using various levels of theory and basis sets. Optimisations in the gas phase and in an implicit polarisable continuum solvent model with a variety of solvents showed that there is a significant dependence of the $I_3^-\cdots I_3^-$ interaction energy on the dielectric constant. We found that the MP2/cc-pVTZ-pp level of theory came closest to reproducing the I_3^- bondlength and the $I_3^-\cdots I_3^-$ intermolecular distance averages obtained from the Cambridge Structural Database (CSD). In addition, MP2/cc-pVTZ-pp results also compare well with the $I_3^-\cdots I_3^-$ interaction energy calculated at the CCSD/aug-cc-pVTZ-pp//MP2/cc-pVTZ-pp level of theory. When considering the I–I bondlength (2.92 Å) in the linear I_3^- ion and $I_3^-\cdots I_3^-$ intermolecular distance (3.80 Å), M06-2X performs best for the former and BP86 for the latter. We found that in general, the 21 density functionals tested (4 GGAs, 11 Hybrid GGAs, 1 meta-GGA and 5 containing DFT-D2 corrections) underestimate the interaction energy, including those with dispersion corrections. However, PBE-D2 gave an interaction energy which is less than 2 % from the CCSD/aug-cc-pVTZ-pp//MP2/cc-pVTZ-pp result.

Keywords Triiodide · PCM model · Anion–anion interaction · Electrostatic · Dispersion

Electronic supplementary material The online version of this article (doi:10.1007/s00214-012-1281-0) contains supplementary material, which is available to authorized users.

F. Groenewald · C. Esterhuysen (✉) · J. Dillen
Department of Chemistry and Polymer Science, Stellenbosch University, Private Bag X1, Matieland 7602, South Africa
e-mail: ce@sun.ac.za

1 Introduction

Triiodides exist in the solid state and in solution as approximately linear molecules which can be symmetric or asymmetric depending on the surroundings. They can generally be formed by mixing an iodide salt (e.g. CsI) with iodine crystals (I_2), similarly to the rest of the polyiodide family where one polyiodide can consist of up to 27 iodine atoms [1–3]. Triiodides are generally found to be disordered in the solid state, and it has been suggested that this disorder may even be dynamic ([2], also [4] and references therein). The bonds found in I_3^- have been referred to as 'secondary bonds', since they are longer (3–4 Å) than a normal I_2 covalent bond. In a theoretical study on the bonding of the I_3^- ion by Kloo et al. [5], the authors came to the conclusion that the formation of these bonds can be adequately described in terms of intramolecular bonding with additional dispersion interactions between the I_2 and I^- fragments. Part of their study looked at the potential energy surface (PES) where they found that the preferred structure for I_3^- in the gas phase is centrosymmetrical ($D_{\infty h}$).

Nuclear Quadrupole Resonance experiments performed by Harada et al. [6] to analyse the triiodide ion's charge distribution in various crystals showed that the symmetric I_3^- ion also has a symmetrical charge distribution where the charges are approximately −0.5 and 0.08 *e* on the terminal and central iodine atoms, respectively. They also found that when the triiodide is asymmetric, the terminal iodine furthest away from the central iodine has the highest charge.

In 1978, Datta et al. carried out a theoretical study on I_3^- by constructing a flexible counterion framework and studying its effects. They showed that the I_3^- ion is symmetric in the gas phase and also in the solid state given a

symmetric counterion environment [7]. Another theoretical investigation mentioned that the asymmetry found in linear anions is strictly related to the surrounding cation distribution in the solid state. Furthermore, the authors pointed out that the orbitals of an I^- ion are stabilised differently depending on the surrounding cation distributions, thus influencing its donor abilities and explaining the asymmetry present in the solid state [8]. This could also explain why there is such a wide range of bondlengths observed for the I_3^- ion in the solid state. Also, previous work has showed that the PES of the $I_2 \cdots I^-$ interaction is very flat and that a small amount of energy is needed to change the bondlength [9].

Some crystals contain one-dimensional $[I_3^-]_\infty$ chains, which have been shown to possess interesting properties such as conductivity [10]. This was verified by a theoretical study performed by Alvarez et al., who proposed mechanisms for the electric conductivity along these $[I_3^-]_\infty$ chains. One method they suggested was ion migration along the chains, which requires little activation since the ions propagate relatively easily through the chain. The authors further pointed out that the hypervalency in I_3^- facilitates ion migration [4]. Another study done by Forsyth et al. [10] showed that polyiodides can be used as doping agents for an insulating polymer matrix, where in some cases, only the I_3^- ion acts as the conducting species. The presence of infinite chains of I_3^- ions in a number of crystal structures, with a variety of cations, suggests that although the surrounding cations in all likelihood play a role in the stabilisation of interactions between I_3^- ions, these $I_3^- \cdots I_3^-$ must be of sufficient strength to direct crystallisation.

Solvent selection has been shown to have a significant influence on the electronic transition energies of trihalides including the I_3^- ion ($\sigma_g \rightarrow \sigma_u^*$ and $\pi_g \rightarrow \sigma_u^*$). These transition energies decrease as the donor ability of the solvent increases either due to the destabilisation of the ground state (σ_g or π_g) or the stabilisation of the excited state (σ_u^*) [11]. Sato et al. found that the free-energy profile of the I_3^- ion in acetonitrile is similar to that found in the gas phase, consistent with experimental results. They did, however, mention that this free-energy profile changes drastically in aqueous solution with an enhanced probability of finding geometries of lower symmetry [12].

In 2006, Clark et al. proposed the existence of a 'σ-hole' on halogen atoms induced by a partially occupied p-orbital, which creates a positive electrostatic potential at the tip of the halogen atom [13]. It has been shown that the potential of the σ-hole plays an important role in formation of the σ-hole bond. Furthermore, the directional nature of the bonding present for σ-holes indicate that it is electrostatic in nature [14]. Another theoretical study done on halogen bonding showed that the positive electrostatic potential of the σ-hole becomes greater if the remainder of the molecule withdraws electron density from the halogen, thus increasing the electrostatic interaction with a particular nucleophile [15]. Halogen bonding has been detected in solution using NMR showing that the solvent has a significant influence on the strength of this intermolecular interaction [16, 17].

Several theoretical studies have been done on electrostatic and dispersion bound complexes where a dependence of the intermolecular interaction on the solvent used was noted. Furthermore, all of these studies yielded consistent results regarding the dependence of a dimer's intermolecular interaction within that dimer on the nature of the solvent [18–23].

In an extensive review article by Svensson and Kloo on the polyiodide series [1], it was shown that the average bondlength and $I_3^- \cdots I_3^-$ intermolecular distance for approximately 500 triiodides are 2.92 and $\geq$3.6 Å, respectively. After this study was conducted, the structures of approximately 280 triiodides added to the Cambridge Structural Database (CSD) have also been found to agree with the results obtained by Svensson and Kloo. Several theoretical studies of the I_3^- ion in gas phase and solution have, however, yielded different results. One study using the PW91 functional with various basis sets in the gas phase calculated bondlengths equal to and greater than 2.97 Å [24]. Other studies found the optimised bondlengths for the I_3^- ion in the gas phase at the HF, MP2, CCSD, CCSD(T) CISD, and QCISD(T) levels of theory to be 2.965, 2.943, 2.964, 2.9822, 2.979, and 3.002 Å, respectively [5, 12, 25].

Furthermore, although the $I_3^- \cdots I_3^-$ interaction has been referred to as a weak interaction [12, 24, 26–33], to our knowledge there have been no studies regarding the qualitative or quantitative nature of this interaction. Therefore, the aim of this study is to understand the driving force behind the formation of $[I_3^-]_\infty$ chains by finding a global energy minimum for a pair of I_3^- ions in a variety of environments and also to study the effect which that the electrostatic environment has on the I_3^- ion and its interactions. In this paper, we report the first step in this process, which is to model the interaction in the presence of a uniform electrostatic field, as experienced in solution. The next step, currently in progress, is to then extend this work to investigate the effect of an anisotropic electrostatic environment as found in a crystal.

Our initial approach was to identify a suitable computational method to adequately describe the experimental structural properties. We therefore tested a large variety of wave function theory (WFT) and Density Functional Theory (DFT) methods in combination with various basis sets. The modelling of these systems was particularly challenging due to the high anion–anion repulsion between the terminal iodine atoms of neighbouring I_3^- ions.

Nevertheless, we are able to report here the computational modelling of the I_3^- ion and its interactions in a variety of solvents, in order to show that the environment plays a significant role in stabilising the $I_3^-\cdots I_3^-$ interaction. We will show that if a sufficient amount of stabilisation energy is provided, highly repulsive electrostatics between anions can be overcome, resulting in attractive interactions. Furthermore, we have identified the driving force making these $I_3^-\cdots I_3^-$ interactions (anion–anion) favourable.

2 Theoretical methods

All calculations were done with the Gaussian 09 rev. B.01 package [34]. All the basis sets used for the calculations were obtained from the EMSL database [35, 36]. Wavefunction theory (WFT) geometry optimisations were performed for the I_3^- and the $I_3^-\cdots I_3^-$ dimers with no symmetry constraints using 2nd-order Møller-Plesset Perturbation theory MP2 [37, 38] in combination with the def2TZVP (dTZ) [39], aug-cc-pVTZ-pp (a-TZ), cc-pVTZ-pp (TZ), aug-cc-pVDZ-pp (a-DZ), and cc-pVDZ-pp (DZ) basis sets [40]. All of these basis sets include an effective-core-potential (ECP) for iodine to decrease the cost of computation and describe the relativistic effects. The Hartree–Fock (HF) interaction energies were obtained by using the MP2 optimised geometry with the same basis set. All calculations were either performed in the gas phase or in an implicit solvation model, utilising the polarisable continuum model [41, 42].

All calculations at the coupled cluster with single and double excitations (CCSD) [43] level of theory were done as single-point calculations for the I_3^- ion and $I_3^-\cdots I_3^-$ dimer using optimised geometries at the MP2/a-TZ level of theory for the gas phase and in ethanol ($\varepsilon = 24.852$) and also water ($\varepsilon = 78.3553$) implicit solvent models. Additional CCSD single-point calculations were performed using optimised geometries at the MP2/TZ level of theory in the chloroform ($\varepsilon = 4.7113$), ethanol ($\varepsilon = 24.852$), water ($\varepsilon = 78.3553$) and *n*-methylformamide-mixture ($\varepsilon = 181.56$). Counterpoise corrections were done only for the gas-phase optimisations [44, 45]. We did not apply this BSSE correction (1.38 kcal/mol for CCSD/a-TZ//MP2/a-TZ) to the solvated ions due to the spurious nature of the stationary point in the gas phase and the magnitude of the $I_3^-\cdots I_3^-$ interaction energy (see Sects. 3.1.2 and 3.1.3).

Density functional theory (DFT) geometry optimisations were performed in gas phase and implicit solvent model using the PBE [46, 47], wB97X [48], wB97XD [49], B971 [50], B97D [51], BP86 [52, 53], B3LYP [54–56], TPSS [57], BLYP [52, 55, 56], PBE0 (PBE1PBE) [58], M06 [59], M06-HF [59], M06-2X [60], LC-wPBE [61–64], B972 [65] and X3LYP [66] functionals in combination with the a-TZ and dTZ basis sets. No symmetry constraints were enforced for the calculations with B97D/a-TZ, TPSS/a-TZ and PBE/a-TZ in methylformamide, which, as with the WFT geometry optimisations, were found to yield symmetric structures, hence the remainder of the calculations were allowed to proceed with inclusion of symmetry. We also incorporated a dispersion correction in the abovementioned functionals as published by Grimme [51], which is denoted by DFT-D2, for example, BP86-D2. The following equations were taken from Grimme's paper and will not be discussed; for further details, see [51].

The Total Energy is given by

$$E_{\mathrm{DFT-D}} = E_{\mathrm{KS-DFT}} + E_{\mathrm{disp}} \tag{1}$$

where $E_{\mathrm{KS\text{-}DFT}}$ is the usual Kohn–Sham energy as obtained by the chosen DFT, and E_{disp} is given by:

$$E_{\mathrm{disp}} = -s_6 \sum_{i=1}^{N-1} \sum_{j=i+1}^{N} \frac{c_6^{ij}}{R_{ij}^6} f_{damp}(R_{ij}) \tag{2}$$

Here, s_6 is the global scaling factor that only depends on the density functional used, N is the number of atoms, c_6^{ij} denotes the dispersion coefficient for atom pair ij given by the equation $c_6^{ij} = \sqrt{c_6^i c_6^i}$ and R_{ij} is the interatomic distance. A damping function is included to avoid near singularities, given by

$$f_{damp}(R_{ij}) = \frac{1}{1 + e - a\left(\frac{R_{ij}}{R_r} - 1\right)} \tag{3}$$

where R_r is the sum of the atomic radii, and a is a constant equal to 20.

The $I_3^-\cdots I_3^-$ interaction energy (E_{INT}) and ΔE_{S} were calculated as follows:

$$E_{\mathrm{INT}} = \mathrm{Energy}\left(I_3^- \cdots I_3^-\right) - 2 \times \mathrm{Energy}\left(I_3^-\right)$$
$$\Delta E_{\mathrm{S}} = \mathrm{Energy}\left(\mathrm{solvated}\, I_3^-\right) - \mathrm{Energy}\left(\mathrm{gas\ phase}\, I_3^-\right)$$

The coordinates, frequencies and energies of the optimised structures are included in the electronic supplementary material.

2.1 CSD searches

Structural data were obtained from the May 2012 update of the Cambridge Structural Database V5.33 utilising the ConQuest V1.14 search program [2]. The search for the I_3^- ion consisted of an I–I–I fragment only. Chains of I_3^- ions were identified by searching for a fragment containing two I–I–I ions with an intermolecular contact less than the sum of the van der Waals distance between the terminal I atoms on the two triiodides. Crystal structures containing I^-, I_2 and polyiodides were excluded. Crystal structures containing chains of I_3^- ions were identified by inspection.

3 Results and discussion

3.1 Wave function theory (WFT)

3.1.1 I_3^- ion bondlength

According to an extensive review article on polyiodides [1], the I_3^- ion decomposes into I_2 and I^- at temperatures equal to or greater than room temperature; thus, it has not been possible to obtain any experimental information on the bondlength of the I_3^- ion other than what has been found in the solid state. However, previous studies have shown that the symmetry of the I_3^- ion in solution is dependent on the solvent used, where the induced asymmetry can facilitate forbidden transitions visible in Raman spectra [3, 67]. This influence of asymmetry on spectra has also been observed in a UV–Vis study on compounds in both the solid state and in solution [68].

Average geometrical parameters for the I_3^- ion obtained from the CSD were reported in 2003; however, since then, there have been approximately 200 additional characterisations of triiodides [1]. We therefore repeated the analysis using the May 2012 update of the CSD [2], where we obtained 787 hits for the discrete I_3^- ion of which only 675 contain bondlength information, and 98 hits for $[I_3^-]_n$, with $n \geq 2$, where 36 form $[I_3^-]_\infty$ chains.

The bondlength of the triiodide ion varies in the solid state from 2.53 to 3.21 Å; however, we found the CSD average to be 2.92 Å. For the intermolecular distance, the CSD average was determined for 36 structures containing $[I_3^-]_\infty$ chains and was found to be 3.8 Å, within a range of 3.58–3.96 Å. Furthermore, considering that less than 5 % of all the structural data available for the I_3^- ion contains structural information for $[I_3^-]_\infty$ chains, the distribution over this range has a low frequency with a global maximum corresponding to the mean.

Previous theoretical studies of symmetrical I_3^- ions in the gas phase at the CCSD and CCSD(T) levels of theory yielded bondlengths of 2.964 and 2.982 Å, respectively [5, 31]. However, the influence of a changing electrostatic environment on the bondlength at these levels of theory was not investigated.

In Table 1, we have summarised the computational results for two geometrical parameters: the I_3^- bondlength and the $I_3^-\cdots I_3^-$ intermolecular distance, with the CSD averages indicated for reference. In addition, the CCSD/a-TZ interaction energy for the I_3^- dimer has been included as a benchmark.

In Table 1, we see that in all cases, the I_3^- ions are calculated as being symmetric, which agrees with previously obtained results [5]. In the gas-phase, MP2 in combination with the dTZ, a-TZ and TZ basis sets gives bondlengths comparable to the CSD average for I_3^- (2.92 Å) with the best result obtained for MP2/TZ (2.921 Å). If the I_3^- ion is placed in ethanol ($\varepsilon = 24.852$) or water ($\varepsilon = 78.3553$), there is a decrease in the

Table 1 CSD averages for the I_3^- bondlength (Å) and $I_3^-\cdots I_3^-$ intermolecular distance (Å), with comparative MP2 geometries from optimisations utilising various basis sets and interaction energies (kcal/mol) at the CCSD, MP2 and HF (in parenthesis) levels of theory

Method	Basis set	Bondlength (Å)			$d(I_3^-\cdots I_3^-)$ (Å)			E_{INT} (kcal/mol)		
		Gas	Ethanol	Water	Gas	Ethanol	Water	Gas	Ethanol	Water
CCSD	a-TZ	–	–					34.381[a,c]	−0.264[a]	−1.279[a]
	a-TZ	–	–					–	**−0.802**[b]	**−1.797**[b]
MP2	dTZ	2.910	2.905	2.905	–	3.637	3.634	–	−1.651	−2.670
								–	(4.940)	(4.024)
	a-TZ	2.924	2.915	2.915	3.901	3.561	3.562	33.170[c]	−3.187	−4.219
								(36.658)[c]	(6.035)	(5.043)
	TZ	2.921	2.912	2.911	–	3.788	3.778	–	−0.769	−1.788
								–	(4.002)	(3.090)
	a-DZ	2.996	2.985	2.985	–	3.786	3.777	–	−1.973	−2.975
								–	(3.896)	(2.989)
	DZ	2.988	2.978	2.978	–	4.018	4.008	–	−0.055	−1.049
								–	(2.538)	(1.594)
CSD average		**2.92 (5)**			**3.80 (10)**			–	–	–

HF interaction energies obtained from MP2 optimised geometries using the same basis set

[a] CCSD/a-TZ//MP2/a-TZ optimised geometry in the gas phase, ethanol and water

[b] CCSD/a-TZ//MP2/TZ optimised geometry in ethanol and water

[c] Counterpoise corrected

Numbers in bold indicate benchmark values used for comparison

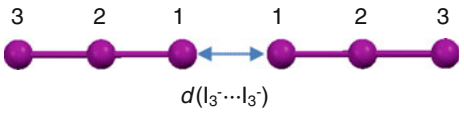

Fig. 1 General geometry of the stationary point found for the I_3^- dimer. Note that $d(I_1–I_2)$ is shorter than $d(I_2–I_3)$, but $d(I_1–I_3)$ is elongated by a negligible amount when compared to a single optimised I_3^- ion

bondlength of approximately 0.01 Å for all basis sets such that the MP2/a-TZ results (2.915 Å in the solvent) are closest to the CSD value. Furthermore, the double-zeta basis sets give elongated I–I distances when compared to the larger triple-zeta basis sets. We believe that this basis set dependence can be attributed to MP2 overestimating the dispersion contribution (see Sect. 3.1.3). This statement is supported by a previous theoretical study of the $I^-\cdots I_2$ bond [5], which identified additional dispersion interactions between the two fragments. However, if one considers that the greatest deviation is only 3 % from the CSD average for the I_3^- bondlength, it is clear that all these basis sets in combination with MP2 perform very well in reproducing the experimental structures.

All of these geometry optimisations yielded symmetrical I_3^- ions, but when optimised as a dimer, the geometries of the individual I_3^- ions are asymmetric, while the total length of the molecule elongates by a negligible amount ($\sim$0.01 Å), see Fig. 1 and Table ESM1 in the electronic supplementary information. Very recently, Aragoni et al. studied triatomic linear molecules and their bondlength deviations in CSD data, where they found that I_3^- has a normalised elongation ($\delta_{I–I}$) $\leq$0.36 when the bondlength d(I–I) is $\leq$3.6 Å. They also calculated the PES for the I_3^- and concluded that the PES is extremely flat and that only a few kilocalories of energy are needed to impose a change in the bondlength [9].

3.1.2 Intermolecular distance $d(I_3^-\cdots I_3^-)$

It is clear from Table 1 that the $I_3^-\cdots I_3^-$ distances deviate much more from the CSD average than the I–I intramolecular distances for I_3^-. This also agrees with what is observed experimentally where the standard deviation for the $I_3^-\cdots I_3^-$ is twice that of the intramolecular I–I bondlength. In the gas phase, only the a-TZ basis set yields a stationary point, which can be attributed to the fact that MP2 overestimates the dispersion interaction. We believe that this stationary point is therefore actually an artefact (see Sect. 3.1.3). Nevertheless, the calculated intermolecular distance (3.901 Å) is slightly greater than the CSD average of 3.8 Å. This slight deviation of the intermolecular distance for the gas-phase dimer from the CSD average can be attributed to the inability of MP2 to model dispersion interactions, thus changing the PES sufficiently to enable us to identify a stationary point. When the dimer is placed in an electrostatic environment, we observe a decrease in the intermolecular distance of 0.34 Å at the MP2/a-TZ level, although the distances are almost identical in ethanol and water. With the other basis sets (except for dTZ), on the other hand, there is a decrease of 0.1 Å in the intermolecular distance in ethanol as compared to water. This decrease in the $I_3^-\cdots I_3^-$ distance in water as compared to ethanol is due to the added stabilisation provided by water as a solvent (see Sect. 4). MP2/TZ reproduces the CSD average most closely. The a-TZ and dTZ basis sets underestimate the intermolecular distance, whereas the double-zeta basis sets overestimate it.

3.1.3 Interaction energy

To our knowledge, there are no experimental or theoretical values available for the $I_3^-\cdots I_3^-$ interaction energy; even a paper on the kinetics of the triiodide ion in aqueous solution using I^{127} NMR, unfortunately, does not report any dimer formation [69]. Thus, we consider the CCSD/a-TZ//MP2/TZ interaction energy to be our benchmark, since CCSD(T)/a-TZ//MP2/a-TZ is computationally too expensive when the dimer is considered.

We have, however, included the CCSD/a-TZ//MP2/a-TZ results in Table 1 due to the substantial dependence of the value obtained for the interaction energy on the geometry used. At the MP2/a-TZ level of theory, the $I_3^-\cdots I_3^-$ distance is shorter than that obtained with MP2/TZ due to the overestimation of the dispersion interaction. The shorter $I_3^-\cdots I_3^-$ distance obtained from the MP2/a-TZ level of theory will result in CCSD/a-TZ giving a less stabilising $I_3^-\cdots I_3^-$ interaction energy. We stress the fact that geometry selection is very important in constructing a benchmark for complexes bound by a shallow PES as a result of electron correlation. The MP2/TZ geometry was used since it was closest to the CSD average.

We found that MP2/TZ delivered an interaction energy of -0.77 kcal/mol with a deviation in ethanol of 5 % from our benchmark of -0.80 kcal/mol. This difference, however, decreased when modelled in a solvent with a higher dielectric constant, resulting in a deviation of just 0.01 kcal/mol from the CCSD benchmark. Our results coincide with a previous study regarding the ability of MP2 to model non-covalent interactions, which concluded that cc-pVTZ-pp gave the most balanced description of the electrostatic and dispersion interactions [70]. It has previously been reported that the ratio of the MP2 and HF interaction energies, ΔE(HF)/ΔE(MP2), can be employed to determine the dominant contributing interaction (electrostatic or dispersion) for various protein–ligand systems [71]. The authors found that when the ratio was positive the

interaction was mainly electrostatic in nature, while a negative value indicated mainly dispersive interactions. The reason for this characteristic is the inability of HF to model dispersion interactions due to the absence of dynamical correlation in the wavefunction [72]. If we now consider the HF interaction energies summarised in Table 1, it can be seen that the interaction appears to remain repulsive regardless of the phase, although the repulsion decreases from 36.7 to 6.0 kcal/mol. Furthermore, the sign of the ΔE(HF)/ΔE(MP2) ratio suggests that the $I_3^-\cdots I_3^-$ interaction in the gas phase is electrostatic, whereas in ethanol and water, the interaction is mainly due to electron correlation. In addition, since the stationary point in the gas phase is considered to be an artefact, the $I_3^-\cdots I_3^-$ interaction has to be studied in a controlled electrostatic environment.

3.2 Density functional theory (DFT)

3.2.1 I_3^- ion bondlength

The variation of the I_3^- ion's bondlength when using various functionals in different polarisable continuum mediums is illustrated in Table 2. It can be seen that all DFT functionals overestimate the average experimental bondlength, except for the M06-HF and LC-ωPBE functionals.

In Table 2, we have included the CSD averages found in Table 1, as discussed in Sect. 3.1.1. We will first focus on the I–I bondlengths obtained for various DFTs with the a-TZ basis set.

The I–I bondlengths calculated using the M06-2X functional are most comparable to the CSD average (2.92 Å), with a deviation of 0.004 Å in the gas phase. The bondlength shortening of 0.008 Å from the gas phase is similar to ethanol and water, irrespective of the electrostatic environment. The ωB97X, PBE0 and LC-ωPBE functionals also give comparable results with deviations less than 1 % from the CSD average. In general, all of the selected DFT functionals perform extremely well with the a-TZ basis set, considering that the largest deviation from the CSD average is less than 5 %.

The dTZ basis set compares well to the a-TZ basis set, but gives slightly shorter bondlengths in each case. Again, the M06-2X functional yields results closest to the CSD average, while PBE0 is also comparable. By comparing the calculated bondlengths to the CSD average, it can be seen that there is a general overestimation of the bondlengths by all the DFT functionals, with the exceptions being the M06-HF and LC-ωPBE functionals. We believe this overestimation of the I_3^- bondlength, seen for the DFT functionals when compared to the CSD average, is a result of the additional dispersion interactions present in the intramolecular bonding of I_3^- [5]. However, reasons for M06-HF and LC-ωPBE giving a shorter I_3^- bondlength than the CSD average are unclear. It can be seen in Table 2 that the BLYP functional yielded the least comparable bondlength (3.049 Å) to the CSD average in the gas phase, with the addition of the D2 correction elongating the I_3^- bondlength even further, thus increasing the deviation from the CSD average.

3.2.2 Intermolecular distance $d(I_3^-\cdots I_3^-)$

As with the WFT methods in Sect. 3.1.1 (Fig. 1), individual I_3^- ions are asymmetric when optimised as a dimer, although the I_3^- ion's total length elongates by a negligible amount ($\sim$0.01 Å) compared to I_3^- (see Tables ESM2 and ESM3 in the online resource). Since, as mentioned before, the stationary point found in the gas phase is an artefact, we did not perform any optimisations of the dimer in the gas phase for the DFT functionals.

Now, let us first consider the intermolecular distance summarised in Table 2 where it can be seen that there is a modest decrease (from 0.001 to 0.108 Å) in the intermolecular distance with the increase in the dielectric constant, with the one exception being BLYP-D2. The average decrease in the $I_3^-\cdots I_3^-$ intermolecular distance (0.014 Å) in ethanol compared to water is consistent with the results for the WFT methods (see Sect. 3.1.2). Three functionals (B972, BLYP and B3LYP) could not describe the PES sufficiently when modelled in ethanol and were unable to identify a minimum. However, when the electrostatic environment was changed to water, the PES changed significantly, enabling us to find stationary points for two (B972 and B3LYP) of these three functionals. Nevertheless, the intermolecular distances at these stationary points are severely overestimated, thus not providing accurate results. This proves that the electrostatic environment influences the PES significantly and that care should be taken when modelling in solvents with relatively low dielectric constants.

The PBE-D2, BP86 and the meta-GGA, TPSS, functionals yield results most comparable to the CSD average for the intermolecular distance, with less than a 2 % deviation with the a-TZ basis set. X3LYP/a-TZ produces results that deviate most from the CSD average for the $I_3^-\cdots I_3^-$ distances with overestimation of 18 and 14 % for the intermolecular distance in ethanol and water, respectively.

A similar dependency of the intermolecular distance on the basis set to that observed for the I–I distances in I_3^- is obtained, where the dTZ results are consistently shorter. Despite this decrease in $d(I_3^-\cdots I_3^-)$, the PBE-D2 functional in combination with the dTZ basis set maintains its less than 2 % deviation from the CSD average for the

Table 2 I_3^- bondlengths (Å), $I_3^-\cdots I_3^-$ distances (Å) and interaction energies (kcal/mol) for various functionals with two basis sets

Method/functional	Basis set	Bondlength (Å)			$d(I_3^-\cdots I_3^-)$ (Å)		E_{INT} (kcal/mol)	
		Gas	Ethanol	Water	Ethanol	Water	Ethanol	Water
CCSD	a-TZ	–	–				**−0.264**[a]	**−1.279**[a]
	a-TZ	–	–				**−0.802**[b]	**−1.797**[b]
PBE	a-TZ	2.976	2.966	2.967	3.705	3.696	0.307	−0.712
PBE-D2		2.978	2.968	2.968	3.856	3.848	−0.813	−1.824
ωB97X		2.943	2.933	2.933	3.925	3.889	−0.435	−1.410
ωB97XD		2.949	2.940	2.940	4.219	4.212	0.202	−0.782
B971		2.965	2.955	2.955	4.063	4.043	0.551	−0.451
B97D		3.029	3.015	3.015	4.003	3.997	−0.600	−1.586
BP86		2.987	2.978	2.977	3.730	3.723	1.100	0.088
BP86-D2		2.990	2.979	2.979	3.887	3.881	−0.517	−1.515
B3LYP		2.994	2.983	2.983	–	4.631	–	0.532
B3LYP-D2		2.997	2.986	2.986	4.034	4.029	0.027	−0.966
TPSS		2.979	2.969	2.969	3.729	3.719	0.961	−0.056
TPSS-D2		2.981	2.971	2.971	3.899	3.886	−0.571	−1.581
BLYP		3.044	3.030	3.030	–	–	–	–
BLYP-D2		3.049	3.036	3.036	3.994	3.995	−0.083	−1.064
PBE0		2.938	2.929	2.929	3.977	3.956	0.832	−0.181
M06		2.972	2.961	2.961	3.927	3.925	−0.173	−1.179
M06-HF		2.841	2.835	2.834	3.880	3.879	1.161	0.113
M06-2X		2.924	2.916	2.916	3.890	3.888	0.234	−0.792
LC-ωPBE		2.898	2.890	2.890	4.361	4.334	1.282	0.316
B972		2.958	2.948	2.948	–	4.505	–	0.286
X3LYP		2.990	2.979	2.979	4.474	4.366	1.293	0.323
PBE-D2	dTZ	2.976	2.965	2.965	3.845	3.838	−0.875	−1.877
BP86-D2		2.988	2.975	2.976	3.881	3.875	−0.551	−1.540
B97D		3.027	3.012	3.012	3.991	3.990	−0.640	−1.616
TPSS-D2		2.979	2.967	2.968	3.894	3.881	−0.624	−1.624
M06-2X		2.922	2.913	2.913	3.881	3.879	0.216	−0.804
PBE0		2.935	2.925	2.925	3.956	3.934	0.782	−0.224
BP86		2.985	2.973	2.974	3.709	3.700	1.056	0.047
TPSS		2.977	2.965	2.965	3.716	3.706	0.901	−0.109
CSD average		**2.92 (5)**			**3.80 (10)**		–	–

CSD average distances and the CCSD/a-TZ interaction energy are included for comparison

[a] CCSD/a-TZ//MP2/a-TZ

[b] CCSD/a-TZ//MP2/TZ

Numbers in bold indicate benchmark values used for comparison

$I_3^-\cdots I_3^-$ intermolecular distance. We did, however, notice that this decrease in intermolecular distance due to the dTZ basis set resulted in the BP86-D2 and M06-2X functionals also yielding comparable results to the CSD average (both 3.881 Å) for the intermolecular distance when considered in ethanol.

We did not notice any substantial dependence of the I_3^- bondlength and $I_3^-\cdots I_3^-$ intermolecular distance on the electrostatic environment, provided the latter is non-directional as is the case with the implicit continuum solvent model. We postulate that any significant changes in the geometry of the I_3^- ion itself or the intermolecular distance between the I_3^- ions can mostly be attributed to the asymmetry of the electrostatic environment, which agrees with what has been found previously (see Sect. 1) [7].

3.2.3 *Interaction energy*

In Sect. 3.1.3, we showed that the attractive nature of the interaction energy is due to the dispersion interaction. The

inability of DFT functionals to model dispersion-type non-covalent interactions has been proven to be the biggest shortcoming of GGA-type DFT functionals although a number of 'remedies' have been proposed to solve this problem (see [73] and References therein). In order to determine whether the $I_3^-\cdots I_3^-$ interaction is similarly poorly modelled, we performed an extensive study testing a variety of DFT functionals. Furthermore, the lack of theoretical data available for the $I_3^-\cdots$ I_3^- interactions required us to expand our investigation to computationally less expensive methods, which can also be employed in quantum mechanical investigations of the I_3^- ion in the solid state.

There is a clear dependence of the interaction energy on the dielectric constant as seen in Table 2, where we have summarised the interaction energies for various DFT functionals. This trend can be observed for all the used DFT functionals where the interaction energy is approximately 1 kcal/mol more attractive in water than in ethanol. We found that the PBE-D2/a-TZ functional yielded an interaction energy within 2 % of the CCSD/a-TZ//MP2/TZ interaction energy in both ethanol and water. Interestingly, when we utilised the PBE-D2 functional with the dTZ basis set, the $I_3^-\cdots I_3^-$ interaction energy became 8 and 4 % more stabilising for ethanol and water, respectively. Although the magnitude of the additional stability calculated with a specific basis set is functional dependent, we found that the E_{INT} is calculated as being stronger when using the dTZ basis set with all the selected DFTs in Table 2 as compared to those obtained with the a-TZ basis set. We are unsure of the reasons for this observed added stability; however, the authors of the dTZ basis set have mentioned that this basis set yields results 'not too far from the DFT basis set limit' [39].

Despite the accuracy displayed by the PBE-D2 functional, we should mention the study carried out by Johnson et al. where they explicitly point out PBE giving 'dispersion-like' binding near minimum energy intermolecular distances which is spurious in nature and is 'directly related to the asymptotic behaviour of the exchange enhancement factor' (see [74] and references therein). We are unsure if the success of PBE-D2 is solely a result of this exchange enhancement factor or only the dispersion correction, or if it is the combination of the two. However, without the D2 correction, PBE underbinds in ethanol by approximately 140 %, which suggests the success is primarily a result of the D2 correction. The only other functionals that perform similarly well to PBE-D2 are the B97D, TPSS-D2 and BP86-D2 functionals, which underestimate the interaction energy in ethanol by roughly 25, 28 and 36 %, respectively. The substantial difference that the inclusion of the D2 correction makes on the calculation of the $I_3^-\cdots I_3^-$ interaction energy is evident when we consider the B3LYP and BLYP functionals, where stationary points could only be identified with the addition of the D2 correction. The addition of a dispersion correction was not successful in every case, however; for instance when we compare the $I_3^-\cdots I_3^-$ interaction energy of the ωB97X (−0.435 kcal/mol) functional to that of the ωB97XD (0.202 kcal/mol) functional with the a-TZ basis set in ethanol, it can be seen that the dispersion correction significantly decreases the accuracy of the method. However, we should mention that the dispersion correction in ωB97XD is identical to the D2 correction with regard to the formula, with the major differences being that the dispersion correction in ωB97XD omits the total scaling factor (s_6) and that the constant a is different, see Eq. 2 and references [49, 51].

4 Dependence of the $I_3^-\cdots I_3^-$ interaction energy (E_{INT}) on the electrostatic environment

As discussed above, the $I_3^-\cdots I_3^-$ interaction energies in ethanol and water summarised in Tables 1 and 2 show a substantial dependence on the environment. In order to further investigate this effect, we have added chloroform ($\varepsilon = 4.7113$) and *n*-methylformamide-mixture ($\varepsilon = 78.3553$) as solvents.

In Table 3, we summarise the $I_3^-\cdots I_3^-$ interaction energies (E_{INT}) and ΔE_S values for our selected solvents, while selected results are represented graphically in Fig. 2.

It is clear from both Table 3 and Fig. 2 that there is a substantial dependence of the $I_3^-\cdots I_3^-$ interaction energy on the dielectric constant. In Table 3, we list results for three WFT methods and three DFT methods with CCSD/a-TZ//MP2/TZ as reference, where we see that the ΔE_S values of the listed methods compare well to one another for a particular solvent. This similarity of ΔE_S values for the various methods suggests that all the methods account for the effect the solvent has on the I_3^- ion, but not necessarily for the $I_3^-\cdots I_3^-$ interaction energy.

In Fig. 2, we have included three WFT methods (CCSD, MP2 and HF) and one DFT functional (TPSS-D2) to demonstrate that both WFT and DFT methods exhibit similar dependence on the dielectric constant even though the E_{INT} differs for a particular method for each of the solvents. For comparison, we have only included data obtained with the a-TZ basis set, although in the Sect. 3.1.3, we concluded that MP2/TZ gives the most comparable results to our CCSD/a-TZ//MP2/TZ benchmark. In Fig. 2, the TPSS-D2 result is shown rather than the better PBE-D2 result for clarity, since the PBE-D2 result exactly overlays the benchmark CCSD result.

In Sect. 3.1.3, we observed that the HF $I_3^-\cdots I_3^-$ interaction energy remains repulsive in both ethanol and water, which is also shown here in Table 3 and Fig. 2 with two

Table 3 E_{INT} and ΔE_S (in italics) (kcal/mol) for chloroform ($\varepsilon = 4.7113$), ethanol ($\varepsilon = 24.852$), water ($\varepsilon = 78.3553$) and *n*-methylformamide-mixture ($\varepsilon = 181.56$) using the a-TZ basis set

Solvent	CCSD[a]	MP2	HF[b]	PBE-D2	TPSS-D2	B97D
	E_{INT} (kcal/mol) and ΔE_S (kcal/mol)					
Chloroform	5.31	3.18	11.89	5.43	5.65	5.50
	−33.16	*−33.11*	*−33.18*	*−33.05*	*−33.28*	*−32.95*
Ethanol	−0.80	−3.19	6.04	−0.81	−0.57	−0.60
	−40.53	*−40.48*	*−40.55*	*−40.47*	*−40.74*	*−40.34*
Water	−1.80	−4.22	5.04	−1.82	−1.58	−1.59
	−41.72	*−41.66*	*−41.73*	*−41.66*	*−41.94*	*−41.72*
n-Methylformamide	−2.06	−4.48	4.78	−2.09	−1.85	−1.85
	−42.03	*−41.98*	*−42.05*	*−41.98*	*−42.26*	*−42.03*

[a] CCSD/a-TZ//MP2/TZ

[b] HF/a-TZ//MP2/a-TZ

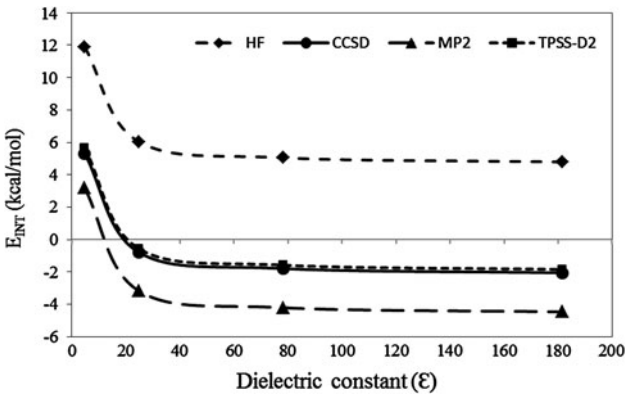

Fig. 2 E_{INT} for the I_3^- dimer in various solvents: chloroform ($\varepsilon = 4.7113$), ethanol ($\varepsilon = 24.852$), water ($\varepsilon = 78.3553$) and *n*-methyl-formamide ($\varepsilon = 181.56$) using the a-TZ basis set

additional solvents (chloroform and *n*-methylformamide). Despite the increase in the dielectric constant to ~181, the E_{INT} (4.78 kcal/mol) for the HF method remains repulsive. Thus, we conclude that the $I_3^-\cdots I_3^-$ interaction energy for HF will always remain repulsive, regardless of the dielectric constant. This is a result of the inability of HF to model dispersion interactions and also proves that highly repulsive electrostatic forces in general can be 'damped'; in particular, the electrostatic forces present between the terminal atoms of the I_3^- dimer.

In Fig. 2, we notice almost identical behaviour exhibited by CCSD/a-TZ and TPSS-D2/a-TZ when E_{INT} is considered as a function of the dielectric constant. Furthermore, the graph suggests that a dielectric constant of ~20 is needed for this interaction energy to become favourable, if the CCSD and TPSS-D2 are considered and approximately 10 if MP2 is considered. As mentioned before in Sect. 3.1.3, MP2 is known to overestimate dispersion interactions which is exposed when the a-TZ basis set is used, as is visible in Fig. 2 for the calculated $I_3^-\cdots I_3^-$ interaction energies.

As mentioned before, a stationary point for the I_3^- dimer in the gas phase can be identified, despite its spurious nature. However, at the CCSD/a-TZ//MP2/a-TZ level of theory, this stationary point is approximately 34 kcal/mol higher in energy than two I_3^- ions at infinite separation. No stationary points were identified at the HF and TPSS-D2 levels of theory. Nevertheless, the repulsive interaction energy of the I_3^- dimer in the gas, despite its spurious nature, provides insight into the severity of the repulsion present without the presence of an electrostatic environment.

To our knowledge, the only previously reported theoretical study on the interactions between ions with the same sign of charge was carried out by Grimme and Djukic [75] in 2011, where they studied cation–cation interactions between rhodium complexes utilising the COSMO solvent model. They pointed out that dispersion corrections are essential when utilising DFT functionals to study these complexes and they concluded that the driving force behind the formation of their doubly charged complex can be attributed to dispersion interactions. Furthermore, they concluded that the repulsion present for the equilibrium structure is 40 kcal/mol, which concurs with our 34 kcal/mol. In an extensive review article written by Pyykkö, in 1996, summarising numerous examples of closed-shell interactions, he concludes that 'When no other obvious bonding contributions exist, one finds at the ab initio level that the attraction is due to correlation effects' [76].

In a theoretical study performed by Aquino et al. [18] investigating the dependence of hydrogen bonding on the solvent used, they concluded that as the dielectric constant increases, the intermolecular interaction decreases. A similar theoretical study was performed by Lu et al. [19] on halogen bonding (X–B) in solution, where they found similar solvent-dependent behaviour to that found for hydrogen bonding. Furthermore, they showed that the X–B

interaction is 1 kcal/mol less stabilising in solvent than in the gas phase. This contrasts considerably with what we found for our study of the I_3^-, where a stabilisation of 35 kcal/mol is provided by the solution if E_{INT} is considered. Gora et al. [20] elucidated the influence of the solvent on intermolecular interactions, where they showed that the observed trend is a result of the decrease in the contribution of the electrostatic interactions to the total interaction energy as the dielectric constant increases. They also mentioned that their results were generally consistent with what Cammi et al. [21] and Contador et al. [22] found for hydrogen bonded complexes. Riley et al. [23] studied interaction energies of biological interest using DFT-D in gas phase and solution where they found a similar dependence of the electrostatic component on the dielectric constant. Furthermore, they investigated the dependence of the interaction energy on the damping parameter (S_R), found in the damping function, where they showed it changed very little from the gas phase to a highly polar environment. However, we should mention that they also studied dispersion bound complexes and found that there is an inverse relation between the dielectric constant and the interaction energy, that is, opposite to our study. Although the $I_3^-\cdots I_3^-$ dimer is an example of a dispersion bound complex, we suspect that this difference is due to the attractive nature of the electrostatic contribution to the total interaction energy. These results are exactly what we are seeing with the $I_3^-\cdots I_3^-$ intermolecular interaction: the electrostatic interaction (repulsive) contribution decreases and as a result the total interaction energy becomes more stabilising.

We believe this trend is applicable to any system where there are repulsive electrostatics present, which is also observed for the cation–cation interactions present in the rhodium complexes investigated by Grimme and Djukic, mentioned earlier [75]. Furthermore, cation–cation and anion–anion interactions have been observed in solution during a study investigating the hydration of oxidised metals and also chloride anions [77].

In Fig. 3, the stabilisation provided by the solvent (ΔE_S) against the dielectric constant is shown, where it can be seen that the behaviour of ΔE_S with the changing dielectric constant is similar to that of the $I_3^-\cdots I_3^-$ interaction dependence. The dielectric constant represents the polarity of the solvent, which is implicitly modelled by surrounding the solute with a polarisable charge distribution, thus the higher the dielectric constant, the higher the electrostatic interaction between the solute and solvent [42]. The similarities in the dependence on the dielectric constant between Figs. 2 and 3 suggest that this increase in stability of the I_3^- ion provided by the solvent decreases the electrostatic repulsion between the I_3^- ions and as a result stabilises the $I_3^-\cdots I_3^-$ interaction. We believe the reason

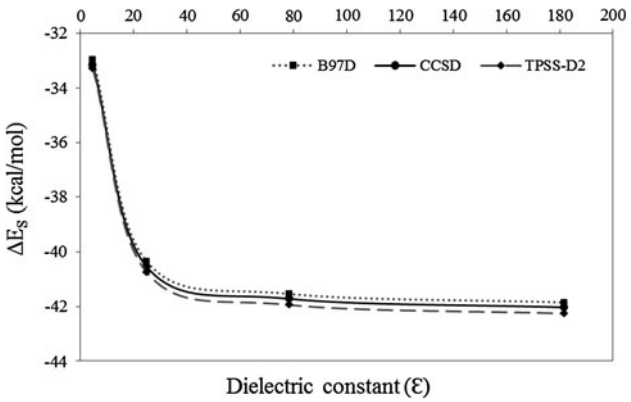

Fig. 3 ΔE_S values for I_3^- in chloroform ($\varepsilon = 4.7113$), ethanol ($\varepsilon = 24.852$), water ($\varepsilon = 78.3553$) and *n*-methyl-formamide ($\varepsilon = 181.56$)

why all the methods listed in Table 3 have similar ΔE_S values lies in the ability of each of the methods to model electrostatic interactions, in particular solute–solvent interactions, which explains the trends seen in both Figs. 2 and 3 (see [23] and references therein).

We mentioned earlier that Fig. 2 shows a dielectric constant of about 20 is needed for this $I_3^-\cdots I_3^-$ interaction to become favourable. In Fig. 3, we can associate the dielectric constant of 20 to a stabilisation (ΔE_S) of about 40 kcal/mol, which is needed for a single I_3^- ion to change the $I_3^-\cdots I_3^-$ interaction from repulsive to attractive. Thus, in solid state, one would expect this stabilisation to be equal to or greater than what is found in a solvent environment. We postulate that if the stabilisation in the solid state is more than what is found for *n*-methylformamide-mixture ($\Delta E_S = 42$ kcal/mol) the E_{INT} will be equal to or less than −2.0 kcal/mol (see Table 3).

5 Conclusions

In conclusion, we used three parameters to measure the performance of various methods, two of which are geometrical parameters determined from experimental structural data contained in the CSD: the I_3^- bondlength [2.92(5) Å] and the $I_3^-\cdots I_3^-$ intermolecular distance [3.80(10) Å], with the third parameter being the $I_3^-\cdots I_3^-$ interaction energy calculated, in selected solvents, at the CCSD/a-TZ//MP2/TZ level of theory. We found that MP2/TZ yields results most comparable to the average values for both geometrical parameters obtained from the CSD, with less than 1 % deviation. Furthermore, MP2/TZ yielded values for the $I_3^-\cdots I_3^-$ interaction energies closest to those obtained at the CCSD/a-TZ//MP2/TZ level of theory, with the greatest deviation from these values being 4 %. This makes MP2/TZ the best performing method for all three parameters defined.

For the DFT results when calculating the I_3^- bondlength and the $I_3^-\cdots I_3^-$ intermolecular distance, M06-2X yielded values closest to the CSD average for the I_3^- bondlength, while for the $I_3^-\cdots I_3^-$ intermolecular distance, PBE-D2, BP86 and TPSS were most successful in reproducing the CSD average for the $I_3^-\cdots I_3^-$ intermolecular distance with a deviation under 2 %. We should mention that with the dTZ basis set, the I_3^- bondlengths and $I_3^-\cdots I_3^-$ intermolecular distances generally decrease when compared to the a-TZ basis set. As might be expected, calculated $I_3^-\cdots I_3^-$ interaction energies become correspondingly more stabilising. If we only consider E_{INT}, we can conclude that PBE-D2/a-TZ comes closest to the benchmark CCSD/a-TZ// MP2/TZ interaction energy in solution, being the only functional that does not underestimate this interaction. However, when we consider the DFT functionals investigated, we notice that there is no one particular method that outperforms the others. However, we should add that we consider the value of the $I_3^-\cdots I_3^-$ interaction energy to be the most decisive parameter in measuring a method's success due to the weak nature and type of this interaction. We thus consider PBE-D2 the most successful DFT functional, given its success in modelling the $I_3^-\cdots I_3^-$ intermolecular distance and interaction energy.

To summarise, we have identified a relatively inexpensive WFT method (MP2/TZ) which is able to successfully reproduce the experimental averages for the I–I bondlength and for the intermolecular $I_3^-\cdots I_3^-$ distance, as well as the $I_3^-\cdots I_3^-$ interaction energy calculated at the CCSD/a-TZ// MP2/TZ level of theory. Furthermore, we were able to identify a few DFT functionals that give comparable results for the geometrical parameters, although only one method yielded a good value for the intermolecular interaction between the I_3^- ions.

Our solvent dependency studies indicated that anion–anion interactions can be favourable in the appropriate environment, and we have identified the minimum amount of energy (ΔE_s) needed, per I_3^- ion, for this interaction to become favourable. The last part of our study showed that the strength of the $I_3^-\cdots I_3^-$ interaction energy converges as the dielectric constant increases, which implies that the attractive interaction energy reaches a maximum regardless of the stabilisation provided by the surroundings.

Although there is no current literature regarding the dielectric constant of a crystalline triiodide-containing compound, we hypothesise that the stabilisation of the I_3^- ion is higher in the (ionic) crystalline environment; consequently, the $I_3^-\cdots I_3^-$ interaction energy will be mostly dependent on the intermolecular distance separating these ions and also the relative orientation in the solid state. We are therefore currently investigating the very important role that the surrounding cations play on the stabilisation of the $I_3^-\cdots I_3^-$ interaction.

Acknowledgments Funding from the NRF through the Competitive Support for Unrated Researchers programme (grant no. 78759) is gratefully acknowledged.

References

1. Svensson PH, Kloo L (2003) Chem Rev 103(5):1649–1684
2. Allen FH (2002) Acta Cryst B58:380–388
3. Loos KR, Jones AC (1974) J Phys Chem 78(22):2306–2307
4. Alvarez S, Novoa J, Mota F (1986) Chem Phys Lett 132(6):531–534
5. Kloo L, Rosdahl J Svensson PH (2002) Eur J Inorg Chem 1203–1209
6. Harada H, Nakamura D, Kubo M (1973) J Magnet Res 13:56–67
7. Datta SN, Ewig CS, Van Wazer JR (1978) J Mol Struct 48:407–416
8. Manca G, Ienco A, Mealli C (2012) Cryst Growth Des 12(4):1762–1771
9. Aragoni MC, Arca M, Devillanova FA, Isaia F, Lippolis V (2012) Cryst Growth Des 12:2769–2779
10. Forsyth M, Shriver DF, Ratner MA, DeGroot DC, Kannewurf CR (1993) Chem Mater 5:1073–1077
11. Detellier C, Laszio P (1976) J Phys Chem 80(22):2503–2506
12. Sato H, Hirata F, Myers AB (1998) J Phys Chem 102:2065–2071
13. Clark T, Henneman M, Murray JS, Politzer P (2007) J Mol Model 13:291–296
14. Mohajeri A, Pakiari AH, Bagheri N (2009) Chem Phys Lett 467:393–397
15. Politzer P, Lane P, Concha MC, Ma Y, Murray JS (2007) J Mol Model 13:305–311
16. Metrangolo P, Panzeri W, Recupero F, Resnati G (2002) J Flourine Chem 114:27–33
17. Bertrán JF, Rodríguez M (1979) Org Magn Res 12(2):92–94
18. Aquino JA, Tunega D, Haberhauer G, Gerzabek MH, Lischka H (2002) J Phys Chem A 106:1862–1871
19. Lu Y, Li H, Zhu X, Liu H, Zhu W (2011) Int J Quantum Chem 112:1421–1430
20. Gora RW, Bartkowiak W, Roszak S, Leszczynski J (2004) J Chem Phys 120:2802–2813
21. Cammi R, Olivares Del Valle FJ, Tomasi J (1988) Chem Phys 122:63–74
22. Contador JC, Aguilar MA, Sánchez ML, Olivares Del Valle FJ (1994) J Mol Struct (Theochem) 314:229–239
23. Riley KE, Vondrášek J, Hobza P (2007) Phys Chem Chem Phys 9:5555–5560
24. Asaduzzaman AM, Shreckenbach G (2009) Theor Chem Acc 122:119–125
25. Danovich D, Hrušák J, Shaik S (1995) Chem Phys Lett 233:249–256
26. Gabes W, Nijman-Meester MAM (1973) Inorg Chem 12(3):589–592
27. Severo A, Gomes P, Visscher L, Bolvin H, Saue T, Knecht S, Flieg T, Eliav E (2010) J Chem Phys 133:064305
28. Saethre LJ, Gropen O, Sletten J (1988) Acta Chem Scand A42:16–26
29. Starikov EB (1997) Int J Quantum Chem 64:473–479
30. Tasker PW (1977) J Mol Phys 33(2):511–518
31. Sharp B, Gellene GI (1997) J Phys Chem 101(11):2192–2197
32. Novoa JJ, Mota F, Alvarez S (1988) J Phys Chem 92:6561–6566
33. Brown RD, Nunn EK (1966) Aust J Chem 19:1567–1576
34. Gaussian 09, Revision B.01, Frisch MJ, Trucks GW, Schlegel HB, Scuseria GE, Robb MA, Cheeseman JR, Scalmani G, Barone V, Mennucci B, Petersson GA, Nakatsuji H, Caricato M, Li X,

Hratchian HP, Izmaylov AF, Bloino J, Zheng G, Sonnenberg JL, Hada M, Ehara M, Toyota K, Fukuda R, Hasegawa J, Ishida M, Nakajima T, Honda Y, Kitao O, Nakai H, Vreven T, Montgomery Jr. JA, Peralta JE, Ogliaro F, Bearpark M, Heyd JJ, Brothers E, Kudin KN, Staroverov VN, Keith T, Kobayashi R, Normand J, Raghavachari K, Rendell A, Burant JC, Iyengar SS, Tomasi J, Cossi M, Rega N, Millam JM, Klene M, Knox JE, Cross JB, Bakken V, Adamo C, Jaramillo J, Gomperts R, Stratmann RE, Yazyev O, Austin AJ, Cammi R, Pomelli C, Ochterski JW, Martin RL, Morokuma K, Zakrzewski VG, Voth GA, Salvador P, Dannenberg JJ, Dapprich S, Daniels AD, Farkas O, Foresman JB, Ortiz JV, Cioslowski J, Fox DJ, Gaussian, Inc., Wallingford CT, 2010

35. Feller D (2007) J Comp Chem 17(13):1571–1586
36. Schuchardt KL, Didier BT, Elsethagen T, Sun L, Gurumoorthi V, Chase J, Li J, Windus TL (2007) J Chem Inf Model 47(3):1045–1052
37. Møller C, Plesset MS (1934) Phys Rev A 46:618
38. Binkley JS, Pople JA (1975) Int J Quantum Chem 9:229
39. Weigend F, Ahlrichs R (2005) Phys Chem Chem Phys 7:3297–3305
40. Peterson KA, Shepler BC, Figgen D, Stoll H (2006) J Phys Chem A 110:13877
41. Tomasi J, Mennucci B, Cammi R (2005) Chem Rev 105:2999–3093
42. Miertuš S, Scrocco E, Tomasi J (1981) Chem Phys 55:117–129
43. Scuseria GE, Schaefer HF III (1989) J Chem Phys 90:3700–3703
44. Boys SF, Bernardi F (1970) Mol Phys 19:553
45. Simon S, Duran M, Dannenberg JJ (1996) J Chem Phys 105:11024–11031
46. Perdew JP, Burke K, Ernzerhof M (1996) Phys Rev Lett 77:3865–3868
47. Perdew JP, Burke K, Ernzerhof M (1997) Phys Rev Lett 78:1396
48. Chai J-D, Head-Gordon M (2008) J Chem Phys 128:084106
49. Chai J-D, Head-Gordon M (2008) Phys Chem Chem Phys 10:6615–6620
50. Hamprecht FA, Cohen A, Tozer DJ, Handy NC (1998) J Chem Phys 109:6264–6271
51. Grimme S (2006) J Comput Chem 27:1787–1799
52. Becke AD (1988) Phys Rev A 38:3098–3100
53. Perdew JP (1986) Phys Rev B 33:8822–8824
54. Becke AD (1993) J Chem Phys 98:5648–5652
55. Lee C, Yang W, Parr RG (1988) Phys Rev B 37:785–789
56. Miehlich B, Savin A, Stoll H, Preuss H (1989) Chem Phys Lett 157:200–206
57. Tao JM, Perdew JP, Staroverov VN, Scuseria GE (2003) Phys Rev Lett 91:146401
58. Adamo C, Barone V (1999) J Chem Phys 110:6158–6169
59. Zhao Y, Truhlar DG (2008) Theor Chem Acc 120:215–241
60. Zhao Y, Truhlar DG (2006) J Phys Chem 110:5121–5129
61. Tawada Y, Tsuneda T, Yanagisawa S, Yanai T, Hirao K (2004) J Chem Phys 120:8425
62. Vydrov OA, Scuseria GE (2006) J Chem Phys 125:234109
63. Vydrov OA, Heyd J, Krukau A, Scuseria GE (2006) J Chem Phys 125:074106
64. Vydrov OA, Scuseria GE, Perdew JP (2007) J Chem Phys 126:154109
65. Wilson PJ, Bradley TJ, Tozer DJ (2001) J Chem Phys 115:9233–9242
66. Xu X, Goddard WA III (2004) Proc Natl Acad Sci USA 101:2673–2677
67. Johnson AE, Myers AB (1996) J Phys Chem 100:7778–7788
68. Gabes W, Stufkens DJ (1974) Spectrosc Chim Acta 30A:1835
69. Myers OE (1958) J Chem Phys 28(6):1027–1029
70. Riley EK, Hobza P (2007) J Phys Chem 110:8257–8263
71. Riley EK, Hobza P (2011) Cryst Growth Des 11:4272–4278
72. Johnson ER, Mackie ID, DiLiabio GA (2009) J Phys Org Chem 22:1127–1135
73. Riley KE, Pitoňak M, Jurečka P, Hobza P (2010) Chem Rev 110:5023–5063
74. Johnson ER, Becke AD, Sherril CD, DiLabio GA (2009) J Chem Phys 131:034111
75. Grimme S, Djukic JP (2011) Inorg Chem 50:2619–2628
76. Pyykkö P (1997) Chem Rev 97:597–636
77. Friedman HL (1988) Faraday Discuss Chem Soc 85:1–11